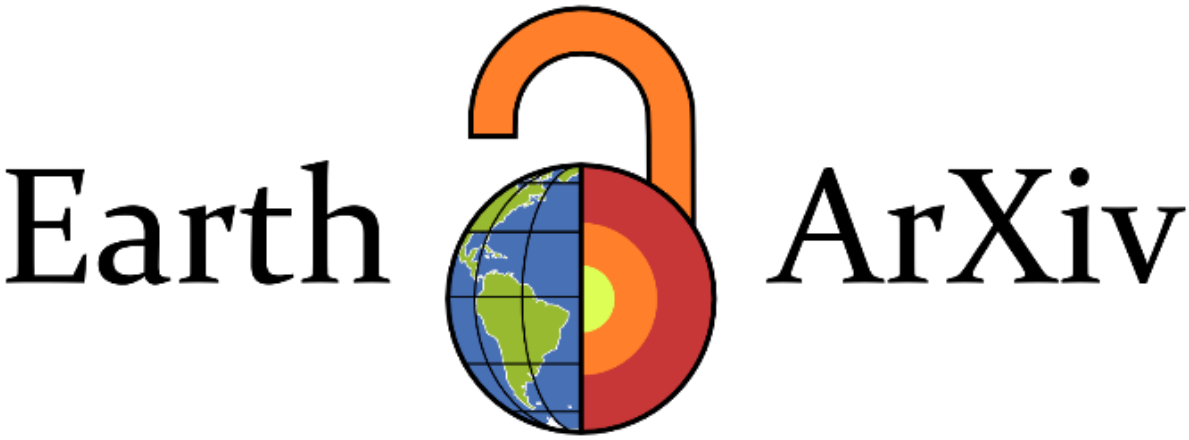

Increasing Floods and Intensifying Droughts: The Future of Hydrological Extremes in a Warming Climate

Chinmay Deval[1], Siddharth Chaudhary[1*]

Chinmay Deval; email: chinmay.deval@uah.edu; ORCID: 000-0002-9492-7602
Siddharth Chaudhary; email: siddharth.chaudhary@uah.edu; ORCID: 0000-0002-8959-8162

[1] Lab for Applied Science, Earth System Science Center, The University of Alabama in Huntsville, 320 Sparkman Drive, Huntsville, AL 35805, USA
* Author to whom any correspondence should be addressed.

Abstract

Understanding how climate change alters the frequency and severity of hydrological extremes is critical for anticipating regional vulnerabilities and guiding adaptation. In this study, we analyze changes in the magnitude, intensity, and duration of extreme streamflow events, both floods and droughts, under RCP4.5 and RCP8.5 scenarios using the FutureStreams dataset. This dataset, driven by multiple CMIP5 climate models, enables a global-scale assessment across all Intergovernmental Panel on Climate Change (IPCC) Special Report on Managing the Risks of Extreme Events and Disasters to Advance Climate Adaptation (SREX) regions. We identified events using percentile-based thresholds derived from historical (1976–2005) streamflow distributions and evaluated future extremes relative to these baselines across seasonal and decadal time slices. Our results show an apparent intensification of extremes, particularly under RCP8.5, with substantial increases in flood and drought events in climate-stressed regions such as South Asia, the Mediterranean, Central Australia, and Northern Europe. The seasonal dynamics of these changes, such as summer drought intensification and winter flood increases, underscore the compound effects of warming, altered precipitation, and snowmelt patterns. While the most significant increases occur in regions with a known history of hydrological stress, some areas with historically moderate variability also exhibit growing extremes, especially toward the end of the century. These findings highlight the urgency of emissions mitigation and region-specific adaptation planning in addressing the increasing risks posed by future hydrological extremes.

Keywords: climate change, Streamflow, hydrological extremes, floods, droughts

1. Introduction

Anthropogenic emissions lead to warming effects both regionally and globally and can significantly alter hydrology. Extensive evidence indicates changes in low, mean, and high streamflows across more than seven thousand gauging stations worldwide (Gudmundsson et al., 2021). These changes have profound implications for aquatic ecosystems, irrigation systems, and critical infrastructure such as dams and water supplies, directly affecting human livelihoods (Falkenmark et al., 2019). According to the Intergovernmental Panel on Climate Change (IPCC), the intensification of the hydrological cycle under various simulated emission scenarios is expected to increase the frequency and severity of extreme events in many regions globally (IPCC, 2021; IPCC, 2023). This presents significant global challenges for water security and water-related disaster risk management.

The future climate projections further suggest an intensified hydrological cycle, with more frequent and severe droughts and floods expected in many regions (Cook et al., 2020; de Brito et al., 2024). These dynamics threaten water availability and amplify risks associated with floods and droughts, which have far-reaching ecological, economic, and social implications. Increasingly, research highlights the importance of compound hydrologic events, where multiple hazards co-occur or sequentially interact, such as prolonged droughts followed by intense rainfall leading to floods (Zscheischler et al., 2020; Raymond et al., 2020) and their impact is often greater than the individual events themselves. Understanding how the future streamflow patterns will evolve, especially in terms of the magnitude, duration, and intensity of extreme hydrological events, is critical for developing adaptive water management strategies to mitigate these impacts and enhance resilience. Elgendy et al, (2024) have discussed several successful adaptive water management case studies, including the reoperation of reservoirs in Quebec, Canada which address snowmelt changes and sustain river flows; community-level adaptations such as water supply regulation in South Africa and smart water utilities in China and ecosystem-based approaches like riparian buffer strips for flood control and mangroves for coastal protection.

Streamflow, a fundamental water cycle component, is influenced by natural and anthropogenic factors, such as shifts in precipitation patterns, increased evapotranspiration, and land use changes. The intensification of wet and dry anomalies in streamflow due to human-induced climate change has been well-documented, with theoretical models and empirical evidence pointing to growing risks of severe droughts and flooding across various regions (Campbell et al., 2011; Zheng et al., 2024). However, many existing investigations, including those that use hydrologic simulations with climate forcings, are geographically restricted to specific regions or watersheds (e.g., Campbell et al., 2011; Gupta et al., 2020; Zheng et al., 2024), constraining the ability to capture broader global patterns of extreme hydrological events. Additionally, studies

that rely solely on in situ gauge data face temporal limitations (e.g., Gudmundsson et al., 2021) due to sparse historical records and uneven global coverage, particularly in low-income or data-sparse regions. The specific research gap this study addresses is the critical need for a systematic, global-scale characterization of the three essential physical dimensions of extreme events: magnitude, duration, and intensity. Existing studies, constrained by regional focus and data limitations, provide insufficient insights into how these key characteristics of future floods and droughts will evolve worldwide under different climate pathways over the coming decades.

Recent advancements in hydrologic modeling and computational capacity have enabled the reliable simulation of streamflow globally, achieving high spatial and temporal resolution while incorporating different future climate scenarios. One such resource is the FutureStreams dataset, which provides globally consistent, high-resolution streamflow projections across multiple emission scenarios (Bosmans et al., 2022). While CMIP6 models (e.g., Eyring et al., 2016) represent the latest generation of climate projections, offering improved resolution and representation of earth system processes, our study leverages the existing FutureStreams dataset, which is derived from CMIP5 outputs. This choice is based on the dataset's utility as a pre-computed and globally validated resource. FutureStreams provides consistent streamflow simulations using CMIP5 models as forcing to the PCR-GLOBWB hydrological model, which has been extensively used and validated for large-scale hydrologic analysis. Recomputing global streamflow projections using the latest generation climate models (i.e. CMIP-6) is a complex and computationally intensive task that is beyond the scope of this paper. However, the FutureStreams dataset offers a robust, consistent foundation required for understating projected evolution of extreme hydrologic events.

The overall motivation of this study is to bridge the gap between large-scale hydrologic modeling and real-world actions, providing robust, globally consistent, and actionable insights into the evolving physical characteristics of hydrological extremes. We build on these advances in computational hydrology by taking the FutureStreams dataset one step further, offering our specific contribution: an in-depth analysis of projected changes in the magnitude, intensity, and duration of extreme streamflow events under the RCP4.5 and RCP8.5 scenarios across diverse global regions. Unlike studies that focus broadly on streamflow trends, our approach isolates and characterizes the dynamics of hydrological extremes to identify high-risk areas and emergent spatial-temporal patterns.

We focus on over 10,000 Global Runoff Data Centre (GRDC) monitoring stations for this analysis. Our primary focus is on extreme hydrological events and their spatial and temporal dynamics through the 21st century under two emission scenarios. Our analysis is specifically designed to transform complex, computationally intensive streamflow projections into actionable insights for extreme flood and drought risk, providing value to practitioners, planners, policymakers, and

community stakeholders seeking data-informed strategies for water management and disaster mitigation.

To enhance the practical relevance of our findings, we also developed an interactive decision-support tool that enables users to explore hydrologic extremes at the station level. This tool delivers percentile-based streamflow metrics and identifies high-risk regions, supporting data-driven actions and decisions for adaptation planning. In line with FAIR principles (Findable, Accessible, Interoperable, and Reusable), the tool facilitates transparency, collaboration, and community resilience.

The overarching goal of this work is to improve global understanding of how hydrological extremes are likely to change in a warming world and to translate that understanding into practical, accessible resources. By combining robust data analysis with decision-oriented tools, we aim to support climate-resilient water management and inform policies that address growing hydrological uncertainty.

2. Methods

2.1. Discharge Data Acquisition and Processing

We used weekly river discharge data from the FutureStreams dataset (Bosmans et al., 2022), which integrates projections from five General Circulation Models (see Table 1) and reanalysis data with state of the art hydrologic model, PCR-GLOBWB (PCRaster Global Water Balance), to produce estimates of future streamflow under various Representative Concentration Pathways (RCP) scenarios. PCR-GLOBWB divides precipitation into rain and snow based on a air temperature threshold (Sutanudjaja et al., 2018; van Beek et al., 2012). Snow then accumulates and is melted based on the air temperature. Here, we used simulated discharge from two RCP scenarios, specifically the RCP4.5 and RCP8.5, to represent a commonly used emissions mitigation scenario and an emissions business-as-usual scenario. The spatial resolution of the FutureStreams data is five arcminutes globally (approximately 10 km at the equator) and it provides aggregated streamflow over weekly time-period. This weekly river discharge data were extracted at the GRDC monitoring stations, with metadata obtained from the GRDC database (GRDC, 2025), ensuring broad spatial coverage across diverse geographical and hydrological settings. To contextualize our findings under different climatic regimes, we used an updated (Iturbide et al., 2020) version of the Intergovernmental Panel on Climate Change (IPCC) climate reference regions initially defined in the Special Report on Managing the Risks of Extreme Events and Disasters to Advance Climate Adaptation (SREX) (IPCC, 2012). Each GRDC station's metadata was spatially joined with the SREX shapefile to assign each station to a standardized climatic region. The spatial distribution of the GRDC stations included in this study and their assignment to IPCC SREX regions is shown in Figure 1.

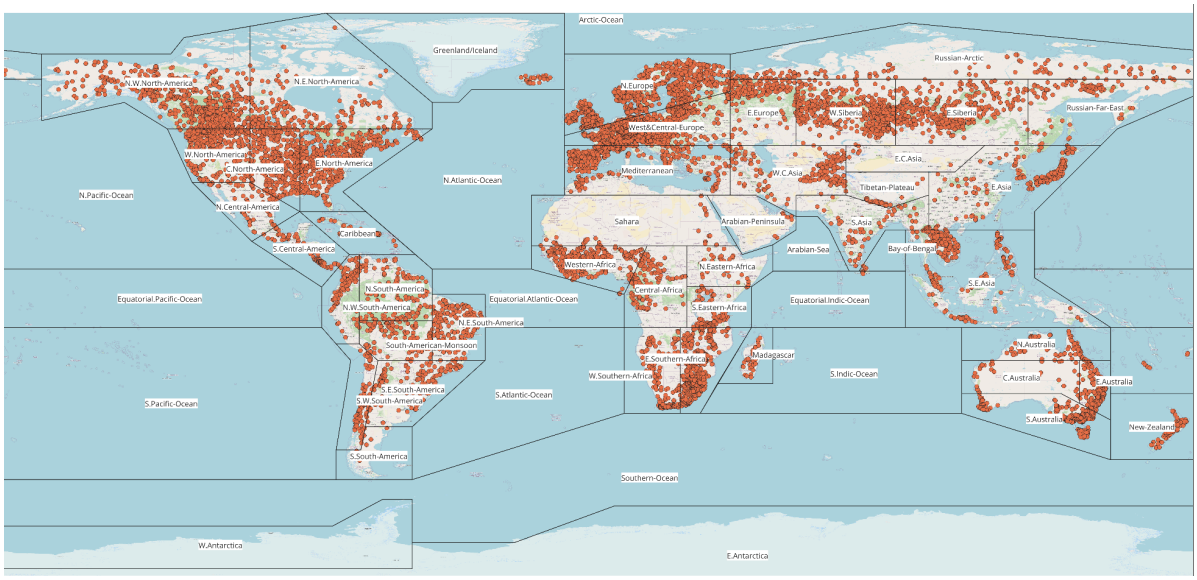

Figure 1: Locations of Global Runoff Data Centre (GRDC) stations used in the analysis, overlaid on IPCC SREX reference regions. Each station is spatially assigned to an SREX region to facilitate regional aggregation and comparative analysis of hydrological extremes.

We analyzed the simulated FutureStreams discharge data created using the five GCMs (GFDL-ESM2M, HadGEM2-ES, IPSL-CM5A-LR, MIROC-ESM-CHEM, and NorESM1-M - see table 1) or two climate scenarios (RCP4.5 and RCP8.5) and reanalysis (Earth2Observe) products across three time frames: historical (up to 2005), and future projections under RCP4.5 and RCP8.5 (2006–2099). These GCMs used to force PCR-GLOBWB for deriving FutureStreams data cover the full envelope of potential climate changes from wet to dry and warm to cold (Warszawski et al. 2013). Future periods were divided into three time slices: early-century (2006–2039), mid-century (2040–2069), and late-century (2070–2099). The median discharge across the five models was calculated for each station and week, providing a robust central estimate and reducing sensitivity to model-specific outliers. This ensemble median time series formed the basis for subsequent analysis and extreme event identification. For extreme hydrologic event identification, we used these weekly values directly. Each weekly streamflow value was compared against historical percentile thresholds (p01 and p99) calculated for each GRDC monitoring station separately. No further aggregation or averaging was applied prior to threshold application. Percentile thresholds (p01 for drought and p99 for flood) were computed independently for each GRDC monitoring station using its historical (1976–2005) weekly streamflow time series. This station-specific approach ensures that thresholds reflect the local hydrological characteristics.

Table 1. CMIP5 Global Climate Models used in the FutureStreams Dataset

No.	GCM Name	Modeling Center
1	GFDL-ESM2M	NOAA Geophysical Fluid Dynamics Laboratory (USA)
2	HadGEM2-ES	Met Office Hadley Centre (UK)
3	IPSL-CM5A-LR	Institut Pierre Simon Laplace (France)
4	MIROC-ESM-CHEM	JAMSTEC, AORI, and NIES (Japan)
5	NorESM1-M	Norwegian Climate Centre (Norway)

2.2. Seasonal classification

To account for seasonal variations in hydrological extremes, each weekly data point was assigned to one of four meteorological seasons based on the calendar month: DJF (December–February), MAM (March–May), JJA (June–August), and SON (September–November). Seasonal groupings were used in later aggregation steps to explore intra-annual patterns in flood and drought characteristics.

2.3. Identification of Extreme Flood and Drought Events

We identified extreme flood and drought events by setting non-parametric thresholds based on historical discharge percentiles. For each monitoring station, we calculated the 1st (p01) and 99th (p99) percentiles from a historical time frame, keeping these thresholds consistent for future comparisons. Several previous studies have used such percentile thresholds in the analysis for characterizing floods and droughts (Matanó et al., 2024; Brunner and Gilleland, 2024; Campbell et al., 2011). Using these p01 and p99 thresholds, evolution in extremes was evaluated against a stable historical baseline. A weekly streamflow was classified as an extreme drought when the discharge dropped below the one percentile threshold, while an extreme flood week was marked when the discharge went above the 99th-percentile flow threshold.

2.4. Event identification, metrics, and analysis

Flood and drought events were defined as contiguous sequences of weeks where discharge remained below (for droughts) or above (for floods) the respective thresholds. For each event, we calculated:

- Duration: Number of consecutive weeks;

- Magnitude: Average discharge anomaly relative to the threshold (p01 minus discharge for droughts; discharge minus p99 for floods);
- Intensity: Magnitude divided by duration, representing the average severity per week.

These metrics were computed for each station and stratified by scenario, time period, and season. Event metrics were aggregated by IPCC SREX regions to assess regional-scale trends. We computed the median event duration, magnitude, and intensity across all contributing stations for each region, season, and time slice. Median values were chosen to reduce sensitivity to extreme outliers and better represent central tendencies in regional-scale hydrological responses.

2.5. Normalization and comparison framework

All comparisons across scenarios and time periods were made relative to historic thresholds, allowing for a consistent frame of reference over time. This approach isolates changes in the characteristics of extreme hydrologic events from baseline variability. As such, differences observed between historical and future periods directly reflect projected changes in climate and hydrological behavior rather than percentile drift. This framework supports robust inter-scenario comparisons and highlights the influence of emission pathways on future flood and drought risks.

2.6. Decision Support Tool

To support stakeholder engagement and practical application of our findings, we developed an interactive, web-based Decision Support Tool (DST). This tool integrates the study's projections of future hydrological extremes into an accessible geospatial platform with an intuitive dashboard interface. The DST utilizes outputs from the analyses of the FutureStreams dataset, specifically the extreme flood and drought frequency and magnitude projections, as described in Sections 2.3 and 2.4. Users can explore projections by selecting combinations of IPCC SREX regions, climate scenarios (RCP4.5 and RCP8.5), and time horizons (early-century, mid-century, and end-century). The core functionality of the DST includes allowing users to view maps of projected changes in hydrological extremes—such as changes in flood or drought magnitude, frequency, and drought duration—as well as to compare projections across different RCP scenarios and time periods through interactive charts and maps. The tool is designed to be user-friendly and accessible to a broad audience, including planners, policymakers, researchers, and community stakeholders. By making complex hydrological projections interactive and interpretable, the DST aims to support informed decision-making for regional climate adaptation.

3. Results

This section presents projected changes in the characteristics of extreme streamflow events—specifically floods and droughts—under RCP4.5 and RCP8.5 scenarios across three future time periods. We focus on three key attributes: duration, magnitude, and intensity, with results aggregated by season and IPCC SREX region to capture both temporal and spatial variation.

3.1. Changes in Flood Characteristics under Climate Change Scenarios

Flood duration exhibits little change in the central tendency across all future periods and scenarios. Median values remain constant at one week, indicating that typical event lengths are largely unaffected. However, a notable expansion in the upper tail of the distribution is observed. The 75th percentile increases from one week in the historical period to two weeks in every future time slice under RCP4.5 and RCP8.5. This suggests that while the majority of extreme flood events retain similar durations, the most prolonged floods could become twice as persistent in future climates (Figure 2a).

In contrast, flood magnitude shows an apparent and progressive increase over time. Under RCP4.5, the median magnitude increased by 40% (~ Δ0.10 cfs) in the early century, 50% (~Δ0.14 cfs) in mid-century, and 58% (~Δ0.17 cfs) in the end century. The upper quartile follows a similar trajectory, increasing to 171% (~Δ2.16 cfs) in the early to 192% (~Δ3.13 cfs) in the mid-century, and reaching 207% (~Δ3.13 cfs) in the late-century period. A comparable but more amplified pattern is evident under RCP8.5, with the median rising by 44% (~Δ0.12) in early century and 81% (~Δ0.3 cfs) by the end-century, and the 75th percentile increasing to 179% (~Δ2.43 cfs) and 258% (~Δ 4.91 cfs) during the same time periods respectively. These trends suggest that not only are extreme floods becoming larger on average, but the most extreme events may exceed three times the historical median (Figure 2b).

Flood intensity also increases consistently through time. Under RCP4.5, the median intensity increases modestly by 23% (~Δ0.03 cfs/week) in the early century and 30% (~Δ0.05 cfs/week) by the end of the century, while the 75th percentile rises to 144% (~Δ1.25 cfs/week) and 158% (~Δ1.55 cfs/week) for the same time periods respectively. RCP8.5 yields a steeper trajectory, with median values increasing from 25% (~Δ0.04 cfs/week) in the early century to 38% (~Δ0.08 cfs/week) in the end century, and upper-quartile values reaching 178% (~Δ2.1 cfs/week) by the end of the century. This trend underscores a future in which floods not only become more prominent but also more forceful over shorter durations, particularly under high-emission scenarios (Figure 2c).

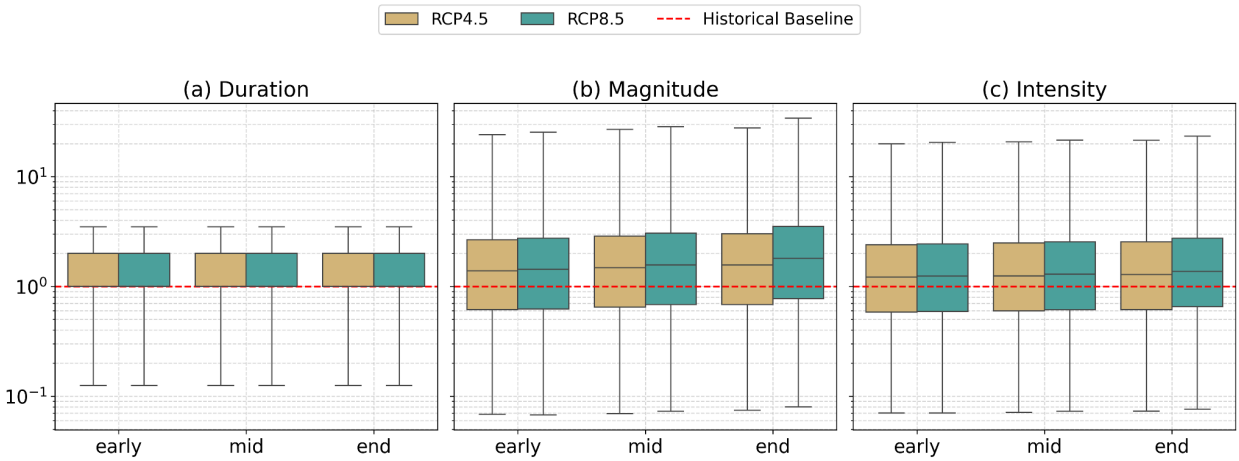

Figure 2: Changes in flood characteristics over time and under different climate scenarios. All metrics are normalized to the station-level historical median values. (a) Flood duration (weeks) shows consistent medians but increasing upper quartiles over time, indicating more persistent extreme events. (b) Flood magnitude (cfs) increases progressively from historical to late-century periods, particularly under RCP8.5. (c) Flood intensity (cfs per week) also increases over time, reflecting more forceful events in future climates. We plot values on a logarithmic scale to highlight distributional variability.

3.2. Seasonal Changes in Flood Characteristics

Flood duration remains stable at the median across all the seasons and time periods relative to the historical baseline. However, the duration in the upper quartile exhibits an increase. Under RCP4.5, the duration of extreme floods in the upper quartile increases uniformly across all seasons from 1 to 2 weeks beginning in the early century and persisting through mid and end-century projections. Similarly, under RCP8.5, a consistent increase to 2 weeks is observed across most seasons and time periods. Notably, in late-century MAM, the 75th percentile extreme flood duration more than doubled, increasing by 1.5 weeks relative to the historic baseline. This signals more frequent, long-duration flood events under the future warming scenarios (Figure 3a)

Flood magnitude demonstrates substantial seasonal and temporal increases. Under RCP4.5, the median magnitude in DJF increased by 41% (~Δ 0.1 cfs) in the early century and reached 62% (~Δ 0.16 cfs) by the end of the century. In JJA, the median increases by 42% (~Δ 0.12 cfs) in the early century and 69% (~Δ 0.27 cfs) in the end century. During MAM, the magnitude increases by 36% (~Δ0.08 cfs) in early-century and 51% (~Δ0.13 cfs) in end-century, and during SON, the magnitude increases peak at 66% (~Δ0.39) by late-century. The 75th percentile magnitude under RCP4.5 also rises markedly, reaching 229% (~Δ 6.23) increase in SON and 244% (~Δ 7.8) increase in JJA by the end of the century. Under RCP8.5, even more significant increases occur:

DJF median magnitude climbs by 91% (~Δ 0.26 cfs), JJA by 100% (~Δ 0.6 cfs), and SON by 92% (~Δ 0.74 cfs) by the end of the century. The 75th percentile magnitudes under RCP8.5 increase to 322% (~Δ 14.39 cfs) in JJA and 284% (~Δ 2.81 cfs) in DJF by the end of the century, indicating substantially stronger extreme floods compared to the historical baseline (Figure 3b).

Flood intensity also displays marked increases across all seasons. Under RCP4.5, median intensity in DJF increases between 20% (~Δ 0.03 cfs/week) in the early century and 27% (~Δ 0.04 cfs/week) in the late century. JJA rises from 28% (~Δ 0.05 cfs/week) early century and 42% (~Δ 0.1 cfs/week) end century, while MAM increases to 16% (~Δ 0.02 cfs/week) early century and 19% (~Δ 0.02 cfs/week) end century. SON increases reach 32% (~Δ 0.1 cfs/week) by the end of the century. The 75th percentile flood intensity under RCP4.5 increases notably to as high as 177% (~Δ 3.1 cfs/week) in JJA and 171% (~Δ 2.86 cfs/week) in SON by the end of the century. Under RCP8.5, flood intensity increases are more substantial: DJF median reaches 33% (~Δ 0.05 cfs/week), JJA hits 62% (~Δ 0.24 cfs/week), MAM 18% (~Δ 0.02 cfs/week), and SON 45% (~Δ 0.21 cfs/week) by the end of the century. Correspondingly, flood intensities in the 75th percentile reach 225% (~Δ 5.27 cfs/week) in JJA and 195% (~Δ 4.73 cfs/week) in SON, further underscoring a growing intensity of flood events, including during the summer and fall months under high-emissions scenarios (Figure 3c).

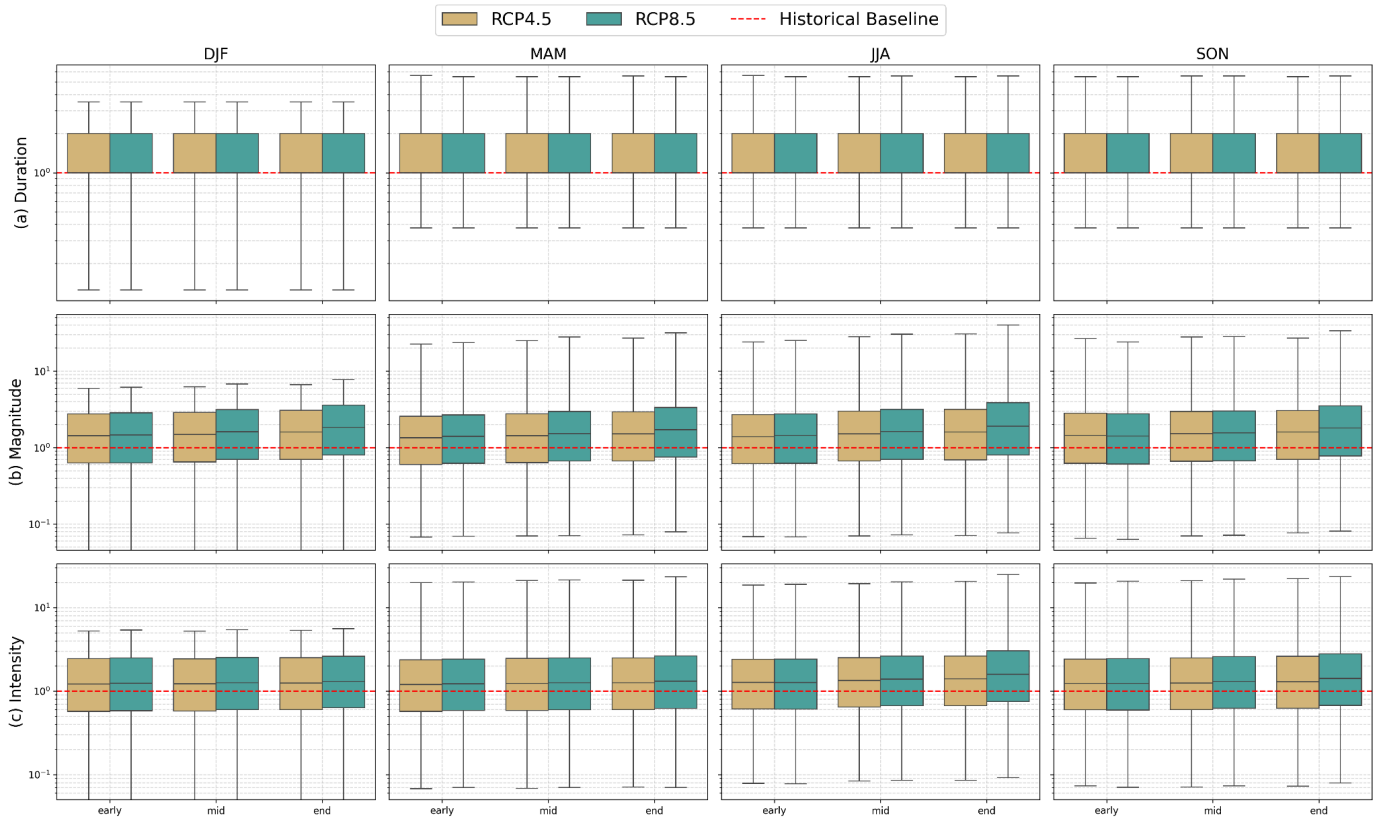

Figure 3: Seasonal changes in normalized flood metrics across future time periods (early: 2006–2039, mid: 2040–2069, end: 2070–2099) and scenarios (RCP4.5, RCP8.5). Each row shows a boxplot distribution of (a) flood duration (weeks), (b) flood magnitude (cfs), and (c) flood intensity (cfs per week) across four seasons (shown in columns): DJF, MAM, JJA, and SON. All values are normalized to the historical median at each station. The red dashed line indicates the historical baseline (value = 1.0). Y-axes are displayed on a log scale.

3.3. Regional Patterns in Flood Duration, Magnitude, and Intensity

The relative change in regional distribution of flood characteristics, specifically duration, magnitude, and intensity across the 21st century under the future climate scenarios RCP4.5 and RCP8.5, is shown in Figure 4. In RCP4.5, regions such as South Asia experienced a marked increase of 33% in median flood duration above the historical baseline. Other regions, including the Arabian Peninsula, N. South America, and N.W. South America showed moderate increases, indicating a regional shift towards more extended flood events. Under RCP8.5, this trend intensified, with South Asia exhibiting a flood duration twice as long as the historical baseline. The Bay of Bengal and Eastern Europe also showed notable increases in flood duration, with the median rising by fifty and thirty-three percent, respectively. These shifts point to a growing risk of prolonged flooding, particularly in regions such as South Asia and the Bay of Bengal, which are critical for agriculture and infrastructure.

Flood magnitude exhibited significant increases across both scenarios. In RCP4.5, regions like the Bay of Bengal, N. South America and South Asia saw flood magnitudes exceed twice the historical baseline. The Bay of Bengal was the most affected, with an increase in flood magnitude reaching approximately 120% relative to the historical median. Other regions among the top five that experienced substantial increases in flood magnitude include N. South America (~100%), S. Asia (~86%), the Tibetan Plateau (~ 78%), and Western Africa (~ 74%) in that order. Under the more extreme RCP8.5 scenario, the flood magnitudes are predicted to continue to rise, with the Bay of Bengal reaching approximately 130% of the baseline. Other regions among the top five that continue to experience an increase in the flood magnitude were the same as those during the RCP4.5 scenario, except for the Russian-Arctic, which is projected to experience about a 97% increase.

Flood intensity followed a similar trend of increasing severity. In RCP4.5, regions such as the S. Pacific Ocean, N. South America, N. Eastern Africa, Russia far east, and C. Australia are among the top five expected to experience significant increases in flood intensity, with intensities ranging between 50-66% above the historical baseline, respectively. Under RCP8.5, this amplification was even more pronounced, with N. Eastern Africa exhibiting the highest intensity,

with the value rising by 73%. C. Australia and the Tibetan Plateau also showed significant increases. Regional median flood metrics across all scenarios are also visualized in heatmap form in Supplementary Figure S1 for completeness. These provide a tabular comparison of relative changes across SREX regions.

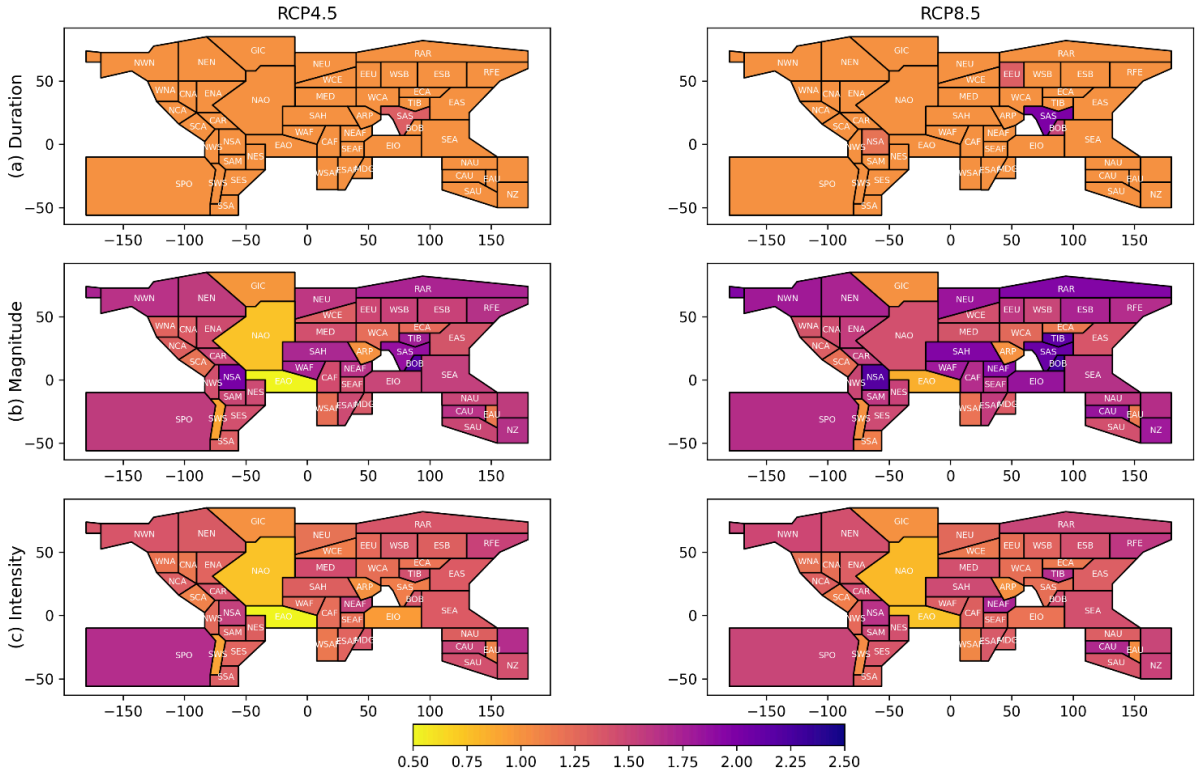

Figure 4: Spatial Distribution of Flood Duration (weeks), Magnitude (cfs), and Intensity (cfs per week) by Scenario across SREX regions.

3.4. Changes in Drought Characteristics Under Climate Change Scenarios

Projected median drought durations remain relatively stable under both climate scenarios, with larger changes towards the end of the century (Figure 5). Under RCP4.5, median drought durations remain stable in the mid and end century, while the drought durations in the upper quartile double during these time periods. Under RCP8.5, drought duration similarly remains stable through the mid-century but increases by 38% by the end of the century. The upper quartile drought duration under RCP8.5 doubles in the mid-century and triples in the end-century.

Drought magnitude is also projected to intensify throughout the century. Under RCP 4.5, the median deficit in drought magnitude increases by 42% (~ Δ0.01 cfs/week) in the early century,

65% (~ Δ0.02 cfs/week) in the mid-century, and 75% (~ Δ0.02 cfs/week) by the end of the century. The corresponding upper quartile deficits range between 167% (~Δ 0.24 cfs/week) in the early century and 234% (~ Δ 0.4 cfs/week) by the end of the century. Under RCP8.5, the median increase in the drought deficit ranges between 48% in the early century to more than doubling by the end of the century. The upper quartile of this deficit increases to 338% (0.77 cfs/week) by the end of the century.

Drought intensity also shows substantial increases. Under RCP4.5, median intensity, relative to historic baseline, increases by 23% in the early century to 40% by the end of the century, with respective upper quartile intensity increasing by 133% (~Δ 0.09 cfs/week) in the early century and 173% (~Δ 0.13 cfs/week) by the end of the century.

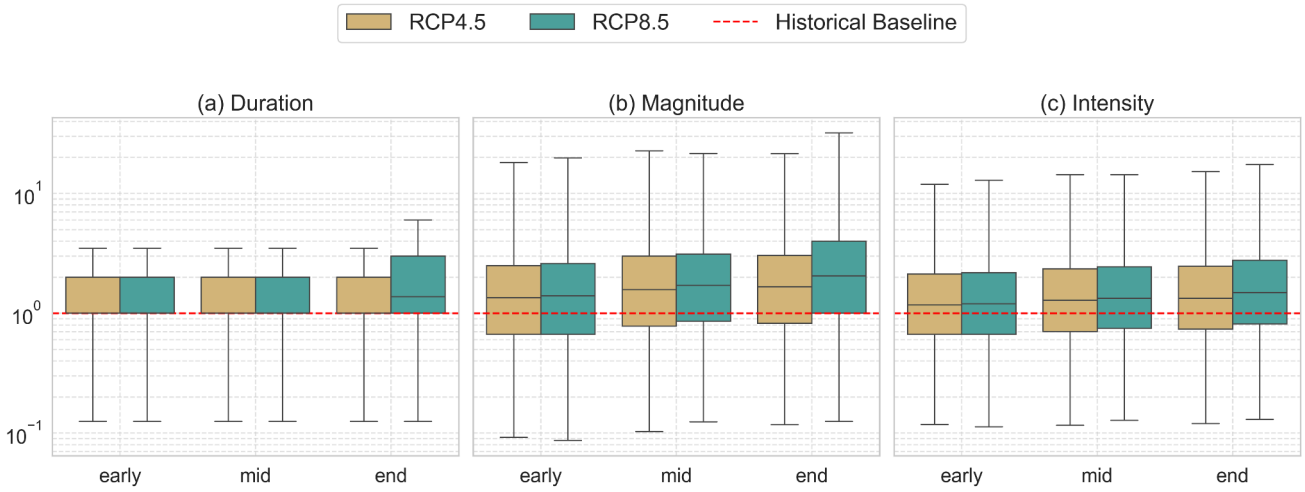

Figure 5. Changes in drought characteristics across future time periods (early: 2006–2039, mid: 2040–2069, end: 2070–2099) and scenarios (RCP4.5, RCP8.5). All metrics are normalized to the station-level historical median values. (a) Drought duration (weeks) shows consistent medians but increasing upper quartiles over time, indicating more persistent extreme events. (b) Drought magnitude (cfs) increases progressively from historical to late-century periods, particularly under RCP8.5. (c) Drought intensity (cfs per week) also increases over time, reflecting more forceful events in future climates. Values are plotted on a logarithmic scale to highlight variability across the distribution.

3.5. Seasonal Changes in Drought Characteristics

Projected seasonal trends in drought duration, magnitude, and intensity exhibit clear departures from historical conditions under RCP4.5 and RCP8.5 scenarios, with stronger responses observed later in the century and under the higher emissions scenario (Figure 6).

Under RCP4.5, median drought duration remains near zero through the end of the century, but the 75th percentile increases across all seasons. By the late century, the 75th percentile reached two weeks in DJF, MAM, and SON, each reflecting a 100% increase from historical values, while JJA drought duration increased by 50% to one week. Under RCP8.5, increases are more pronounced. By the end of the century, median durations increased by approximately 1 week in DJF (33%), MAM (33%), and SON (50%), with JJA increasing by 0.5 weeks (20%). The 75th percentile increases to 3 weeks in DJF, MAM, and SON, representing 200% increases and 2 weeks in JJA (+200%).

Drought magnitude also increases across all seasons. Under RCP4.5, median deficit values increased modestly by the late century to 0.025 cfs in DJF (100%), 0.01 cfs in MAM (65%), and 0.02 cfs in SON (70%). The 75th percentile increases in drought deficit are more substantial, with DJF deficit reaching 0.82 cfs (+328%), MAM reaching 0.35 cfs (+239%), and SON reaching 0.41 cfs (+224%). Under RCP8.5, drought magnitude intensifies significantly. By century's end, median deficit values increased to 0.06 cfs in DJF (134%) and SON (120%), with MAM and JJA also showing substantial increases. At the 75th percentile, DJF deficit reaches 1.44 cfs (476%) and SON 0.745 cfs (327%).

Drought intensity follows similar seasonal patterns. Under RCP4.5, end-century 75th percentile values increase to 0.19 cfs/week in DJF (200%) and 0.13 cfs/week in SON (150%). Median values remain stable in all seasons relative to the historic baseline, indicating that intensification is most apparent during extreme events. Under RCP8.5, drought intensities rise further. By the late century, the 75th percentile reached 0.245 cfs/week in DJF (215%) and 0.16 cfs/week in SON (170%). MAM and JJA also increase to 0.15 and 0.07 cfs/week, respectively. Median intensities climb slightly to 0.01 cfs/week in DJF, MAM, and SON, reinforcing that the most severe droughts are becoming disproportionately more intense.

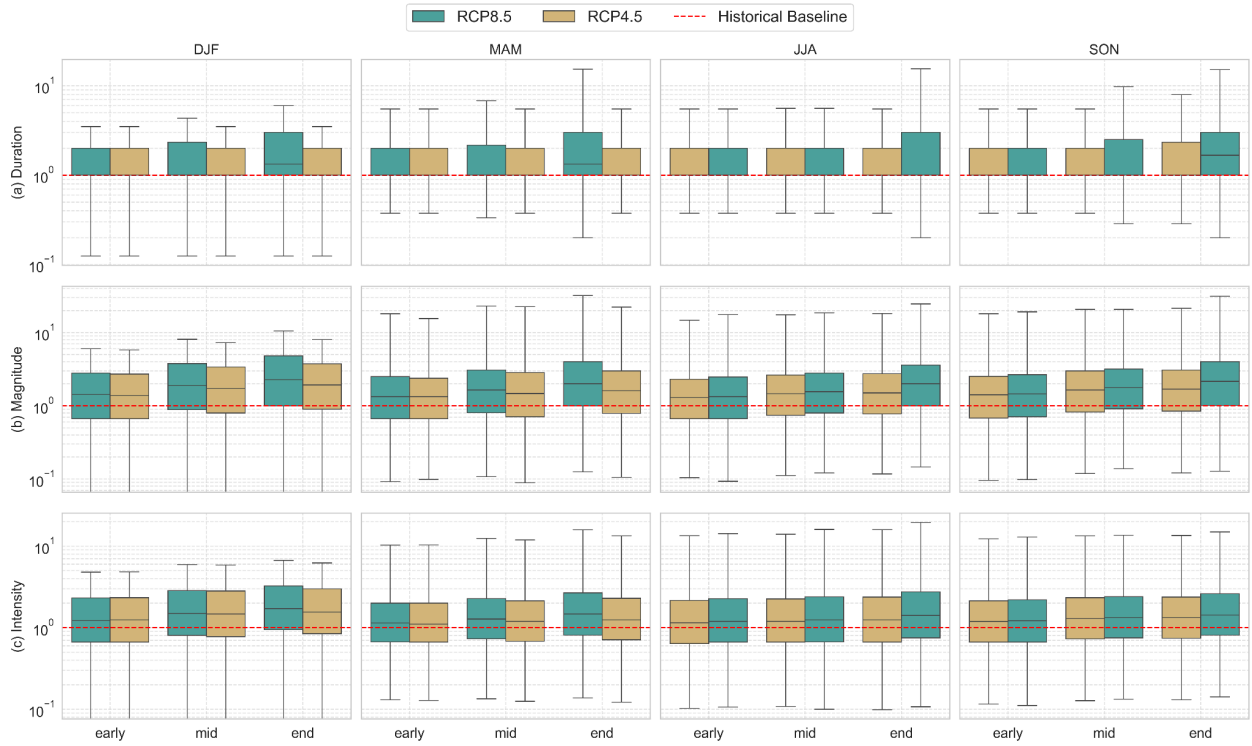

Figure 6: Seasonal changes in normalized drought metrics across future time periods (early: 2006–2039, mid: 2040–2069, end: 2070–2099) and scenarios (RCP4.5, RCP8.5). Each row shows a boxplot distribution of (a) drought duration (weeks), (b) drought magnitude (cfs), and (c) drought intensity (cfs per week) across four seasons (shown in columns): DJF, MAM, JJA, and SON. All values are normalized to the historical median at each station. The red dashed line indicates the historical baseline (value = 1.0). Y-axes are displayed on a log scale.

3.6. Regional Drought Patterns Across SREX Regions

The relative change in the regional distribution of drought characteristics, specifically duration, magnitude, and intensity under the future climate scenarios RCP4.5 and RCP8.5, is shown in Figure 7. Under RCP 4.5, several regions exhibited a considerable increase in drought severity. South America, especially N.E., N., and S.W. South America, along with the South American Monsoon region, experienced a substantial increase of 50-100% in drought duration values as compared to the historical baseline and an increase in magnitude by 110-150%. Southern Australia also showed considerable increases, with particular rises in drought magnitude by more than 120% from the historical values. Drought severity accelerated significantly in regions such as Eastern Central Asian and Northern Australia, where severity doubled or even tripled relative to the baseline, implying a shift towards more extreme dry periods even under

moderate warming scenarios. The Sahara also shows amplified drought characteristics on multiple metrics.

In contrast, several high-latitude and oceanic regions, such as the Tibetan Plateau, Russian Arctic, and South Pacific Ocean, show relatively muted responses, with changes remaining near historical levels across all drought characteristics.

Under the more extreme RCP8.5 scenario, regional disparities became more pronounced. The Sahara emerged as the most dramatically affected region, with drought magnitude exceeding 3.5 times and intensity surpassing 2.5 times historical levels. Similarly, the South American Monsoon zone, Northern and S.W. South America, and Madagascar exhibited sustained high increases in drought duration (100%) and magnitude (>200%). The Mediterranean region also saw a marked rise in drought duration, moving into the high-risk category under RCP8.5. An interesting anomaly occurred in the Bay of Bengal (BOB), where drought duration and magnitude slightly decreased, but drought intensity still doubled, suggesting the potential for shorter yet more severe drought episodes, likely driven by shifts in monsoon behavior.

While certain regions, particularly across the Arctic and Siberian zones, remained relatively stable under both scenarios, the widespread intensification observed under RCP8.5 highlights the amplifying effect of high emissions. Notably, many drought hotspots were already evident under RCP4.5, indicating that increased drought risk is not solely a feature of extreme warming but a robust pattern across emission scenarios.

For completeness, regional median drought metrics across all scenarios are visualized in heatmap form in Supplementary Figure S2, providing a detailed comparison of relative changes across SREX regions. Together, Figure 6 and Figure S2 underscore the critical role of regional context in understanding and addressing future drought risks and illustrate the significant potential for climate mitigation to constrain both the extent and severity of drought impacts, particularly in vulnerable areas.

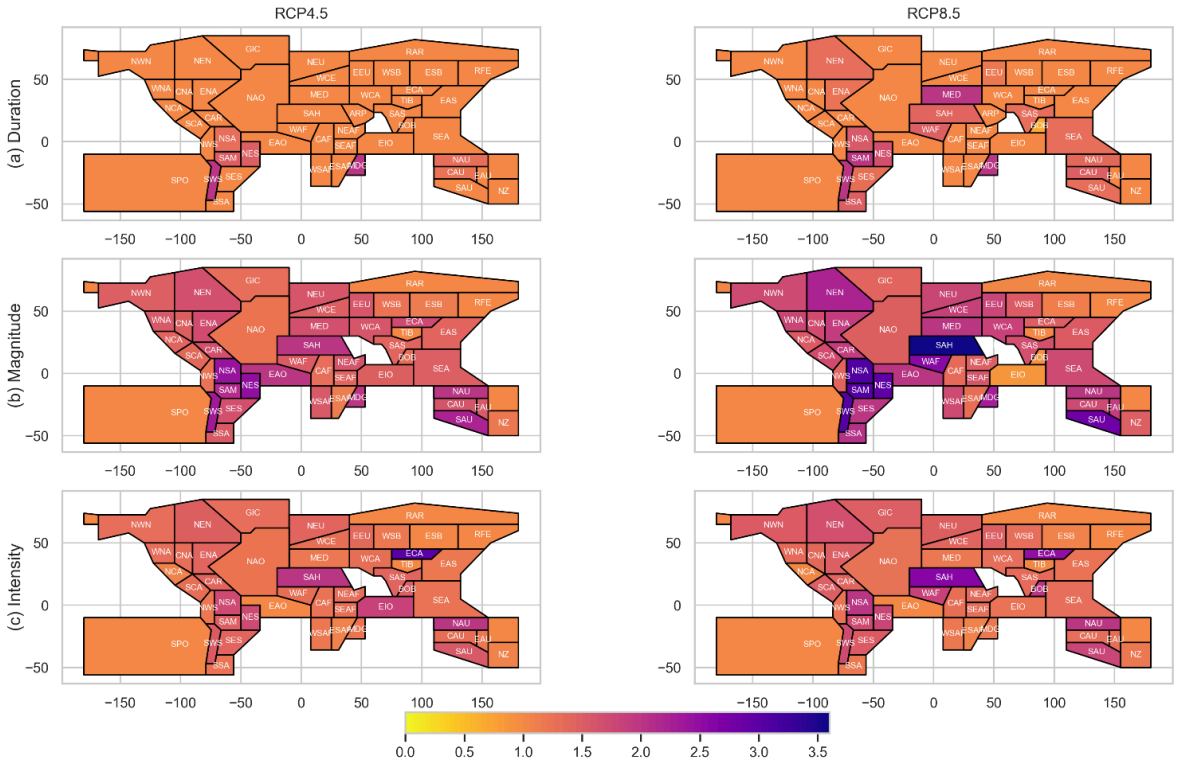

Figure 7: Spatial Distribution of Flood Duration (weeks), Magnitude (cfs), and Intensity (cfs per week) by Scenario across SREX regions.

4. Discussion

Understanding the evolution of future hydrological extremes is essential for anticipating water-related risks in a warming world. While past studies have laid a foundation by capturing historic trends in streamflow and hydrological variability, offering local-scale information about flood and drought risk (e.g., Hirabayashi et al., 2013; Dankers et al., 2014), our study leverages the high-resolution, globally consistent FutureStreams dataset to provide an assessment of future hydrological extremes for all SREX regions. By using FutureStreams, which integrates multiple GCMs, and focusing on both RCP4.5 and RCP8.5 emissions pathways, we provide a systematic, comparative examination of evolving extreme hydrologic floods and droughts at a global scale.

Our results align with conventional knowledge, particularly within the high-emissions RCP8.5 scenario, showing a marked intensification in both hydrologic flood and drought extremes. Moderate but substantial changes in RCP4.5 mean even small mitigation would be unable to offset hydrological hazards, significantly in vulnerable locations. This agrees with earlier findings

identifying increased drought risk in dry and semi-dry areas like the Mediterranean, Central Australia, and South Asia, and greater flood possibility in higher-latitude areas owing to changes in snowmelt timing and precipitation patterns (Hirabayashi et al., 2013). Our findings for the South Asia region, for example, which indicate an increase in both flood and drought extremes, are consistent with similar regional-scale studies climate models. Research focusing specifically on Pakistan confirms a projected intensification of climate extremes and spatiotemporal trends, particularly under high-emission scenarios (Khan et al., 2023). These studies also highlight the significant influence of large-scale climate variabilities, such as monsoonal patterns, on regional precipitation and subsequent hydrological extremes (Hussain et al., 2022). Furthermore, our results align with recommendations for policy to address future climatic changes and related uncertainties in sub-regions like the Hindu Kush, emphasizing the need for robust planning and adaptation (Ali et al., 2021).

A key contribution of our analysis is the identification of emerging hotspots of hydrological extremes. The South American continent stands out as a hotspot of multi-hazard vulnerability, with the South American Monsoon region, N.E. South America, and S.W. South America among the most vulnerable on both flood and drought indices. The convergence of high drought duration and flood severity in these areas reflects increasing exposure to compound and alternating hazards with extensive implications for water management, agriculture, and disaster resilience. Other emerging concern zones include Eastern Central Asia and the Sahara, where drought magnitude is projected to triple relative to historical baselines. At the same time, flood magnitude increases sharply, raising alarm on cascading ecological and societal impacts.

Conversely, some regions break away from the typical patterns. The BOB, for example, shows enhanced flood severity but relatively short-lived drought periods under RCP8.5, which implies leaning towards heavy, short-duration rainfalls. Conversely, cold regions such as the Tibetan Plateau and Russian Arctic have minimal projected change, possibly due to model limitations or extreme baseline conditions dominating incremental changes. These findings emphasize the importance of placing projections into context, both in terms of climatological baselines and model capability.

In addition to single-point extremes, our results reveal a growing dominance of compound hazards in regions suffering from intensifying flood and drought risk. It is mainly for South American and Eastern Central Asian lands, where composite drought-flood processes can enhance vulnerability, destabilize seasonal water availability, and diminish the efficiency of traditional risk reduction strategies. It shows the need for coordinated planning to address the complex interaction of hydrological extremes. It also points toward the possibility of cascading processes, such as long-term dry spells followed by an intense spell of rain.

Seasonal patterns also show the spatial heterogeneity of future change. In high-latitude regions, such as Northwest North America (NWN) and Northern Europe (NEU), more extreme flood events are expected during winter and spring seasons in Mediterranean (MED) and Central Australian (CAU) areas in response to a transformation to rain-driven rather than snow-driven hydrological regimes. Alternatively, in Mediterranean and central Australian catchments, drought risk elevates in extreme summer and autumn periods that are historically low in flows and of high concern for water demand and ecosystem stress.

While this study provides robust insights, several limitations merit acknowledgment. First, the projections rely on CMIP5-based climate forcings embedded in the FutureStreams dataset. We recognize that CMIP6 models (Eyring et al., 2016) represent the current state-of-the-art in climate modeling, offering notable advancements in model resolution, complexity, and the representation of Earth system processes. While CMIP6 models often project slightly stronger warming and exhibit a reduced inter-model spread for temperature and precipitation compared to CMIP5 (Martel et al., 2022; Hausfather et al., 2022), the implications for hydrological extremes in the literature are more nuanced, showing both areas of consistency and divergence. On one hand, several studies suggest a general consistency in large-scale trends. For instance, Lei et al. (2023) largely confirm the overarching direction of projected changes in mean and peak streamflow between CMIP5 and CMIP6. Martel et al. (2022), in their comparison of hydrological impacts over North America, found that while CMIP6 yields a narrower band of uncertainty for future flow values, the overall patterns of change, particularly for extreme events, remain largely consistent with CMIP5 projections. Similarly, Zhang and Chen (2021), in their global analysis of precipitation and temperature extremes, demonstrated that the inter-model spread within CMIP5 for precipitation and subsequent streamflow extremes frequently overlaps with that of CMIP6, especially at regional scales. On the other hand, some regional studies highlight significant differences. For example, Aguayo et al. (2024), focusing on hydrological droughts in the Southern Andes, found "significant climatic (greater trends in summer and autumn) and hydrological (longer droughts) differences" between CMIP5 and CMIP6 projections for their specific region. Additionally, CMIP6 has been identified to potentially perform superiorly for certain regional projections, particularly for drought (Zhai et al., 2020; Gupta et al., 2020), which can lead to deviations in projected magnitudes or specific event characteristics. Despite these regional deviations and evolving model capabilities, the large-scale spatial validation of the historical simulations in the FutureStreams dataset at 3000 GRDC sites (Sutanudjaja et al., 2018) ensures high confidence in the robustness of the underlying hydrological simulations for capturing broad patterns and providing valuable insights into the general direction of future changes. We acknowledge that a full and rigorous assessment of the model's ability to capture historic extreme floods and droughts is challenging

due to insufficient observational data, a point also noted by Van der Wiel et al. (2019). Therefore, while acknowledging these nuances and the evolving landscape of climate modeling, our reliance on the globally consistent FutureStreams dataset still enables robust analysis of broad-scale shifts in hydrological extremes. Future research should ideally leverage emerging CMIP6-driven global hydrological products to refine regional assessments and explore these differences in greater detail. Second, we employed fixed historical percentile thresholds (p01, p99) to define extremes, facilitating consistent cross-scenario comparison. This approach was chosen to quantify the projected exceedance of historically defined extreme conditions, which is a crucial metric for assessing the vulnerability of existing infrastructure and societal adaptation plans built on historical design standards. This method provides a consistent frame of reference, allowing for direct comparison of the projected exceedances of historical extreme conditions across different warming scenarios. However, under ongoing warming change, the assumption of stationarity in hydrological processes is increasingly violated (Milly et al., 2008). This non-stationarity means that historical relationships and thresholds may no longer apply, potentially causing our approach to underrepresent evolving baseline conditions and future risks. We acknowledge that a standardized streamflow index (e.g., SSI) is a more robust approach for cross-site comparisons; however, our use of absolute units was a deliberate choice to provide a direct and tangible measure of how a future hydrograph is projected to behave relative to its historical extremes, which is a key requirement for informing regional water resource management and engineering applications. Consequently, recent studies are exploring adaptive thresholding methods or standardized indices (e.g., SSI) that normalize for varying climatic conditions, offering a more robust framework for identifying and comparing extremes across different warming scenarios (Li et al., 2024). Future research, building upon our global insights, should aim to explore the application of such adaptive methodologies to provide more dynamically relevant assessments of hydrological extreme risks in a non-stationary world.

Third, while our analysis identifies regions prone to intensifying flood and drought risks and conceptually discusses the emergence of compound hazards, this study does not include a quantitative or methodological treatment of co-occurring or sequential drought-flood events. A structured identification of compound event behavior, such as using transition probabilities or specific temporal windows, falls beyond the scope of this assessment of individual extremes and would require dedicated methodological development and extensive additional computations (e.g., Zscheischler et al., 2020; Raymond et al., 2020).

Fourth, this study does not account for human interventions, such as reservoir operations, dam regulations, water withdrawals, or upstream water management, which possess high potential to alter streamflow patterns, especially in strongly regulated basins. Our reliance on a global hydrological model without explicit human water management modules means that projected

streamflow, particularly in strongly regulated or highly utilized basins, may deviate from observed realities. For instance, in regions with extensive reservoir infrastructure, our flood peak projections might be overestimated as reservoir operations typically attenuate flood events, while drought conditions could be underestimated if reservoir releases for supply are not captured. Conversely, in areas with significant water withdrawals for agriculture or industry, our simulated low flows and drought severities might be underestimated. Future work should strive to integrate these critical anthropogenic influences, perhaps by employing advanced hydrological models that incorporate reservoir operation rules or by coupling with water management models. Datasets like the Global Reservoir and Dam Database (GRanD) (Lehner et al., 2011) offer valuable information to support such efforts and enable a more realistic assessment of future hydrological extremes under both climatic and anthropogenic pressures. Additionally, while we acknowledge inter-model variability and structural uncertainty (Zhang and Chen, 2021; John et al., 2022), quantifying these uncertainties was beyond the study's scope. It is important to note that a more detailed analysis of extreme events on a model-by-model basis would provide a more nuanced view of the full range of potential impacts, and is therefore a critical avenue for future research.

Overall, this study expands the existing knowledge of future hydrological extremes in a strong scenario-based assessment of all SREX regions. Divergence and convergence in flood and drought patterns, identification of regional hotspots, compound hazards, and seasonality issues are some emerging results that highlight future research directions. Future studies can build upon these results by including CMIP6 models, socio-economic and infrastructure data integration, and adaptation alternatives for reducing climate vulnerability.

5. Conclusions

This study highlights the significant regional variability in the frequency, intensity, and duration of extreme drought and flood events under different climate scenarios. Our findings show that regions already vulnerable to extreme events, such as South Asia and South America, are expected to experience a marked increase in drought and flood extremes under the RCP8.5 scenario by the end of the century. The MAD, CAU, and parts of Eastern Central Asia also show heightened drought risk. At the same time, NEU and NWN exhibit increased flood occurrences, particularly in the winter and spring, due to altered snowmelt and precipitation dynamics. These results underscore the heightened vulnerability of these regions to future climate impacts, emphasizing the critical need for targeted adaptation strategies that address both seasonal extremes and long-term trends.

The analysis further reveals the emergence of new vulnerabilities in regions previously considered stable or less susceptible to extreme weather. For example, the BOB and certain

tropical monsoon regions show rising flood risks, while areas such as the Sahara experience increasing drought intensity alongside flood magnitudes. These shifting patterns signal a broader distribution of climate risk and emphasize the need for proactive monitoring and preparedness in regions that may not have traditionally been the focus of extreme climate events.

Our comparison between the RCP4.5 and RCP8.5 scenarios underscores the critical role of emissions mitigation in managing the frequency and severity of extreme climate events. As expected, lower-emission scenarios (RCP4.5) show significantly fewer extreme events, highlighting the benefits of reducing greenhouse gas emissions. Such efforts will play a pivotal role in limiting the intensity of future extremes and ultimately mitigating the negative impacts on vulnerable populations, ecosystems, and regional economies. Immediate and substantial reductions in emissions are essential for limiting climate risk and preventing a potential cascade of compounding extreme events.

The study also reveals an increase in drought frequency, particularly in water-stressed regions such as the Mediterranean and Central Australia, which are increasingly vulnerable to prolonged dry spells and reduced rainfall, particularly during the summer (JJA) and fall (SON) months. This highlights the growing susceptibility of these regions to future water scarcity. In parallel, flood risks are rising across diverse regions, with tropical and monsoon-affected areas, like South Asia, experiencing substantial increases, especially in the summer (JJA) and post-monsoon (SON) seasons. This is primarily driven by increased rainfall and shifting precipitation patterns, exacerbating the flood threat in these regions.

In temperate regions like NWN and NEU, flood occurrences rise during winter (DJF) and spring (MAM) seasons, partly due to warming-induced changes in snowmelt timing and precipitation variability. These shifts emphasize the need for region-specific adaptation strategies to manage the compounded risks of floods and droughts, with enhanced water management strategies, flood forecasting, and drought preparedness becoming central to future resilience planning.

In conclusion, this study underscores the importance of understanding regional climate dynamics and the impact of different emissions scenarios on the frequency and severity of extreme weather events. As regions face a growing array of hydrological extremes—often occurring together in compound events—immediate action to mitigate emissions, coupled with comprehensive adaptation measures, is crucial to address the growing risks posed by climate change. While our study provides a systematic global assessment of individual flood and drought extremes and identifies regions of multi-hazard vulnerability, a detailed quantitative analysis of the specific spatiotemporal dynamics and transitions of compound hydrological

events remains an important area for future research. Tailored strategies are needed to safeguard vulnerable populations, ecosystems, and infrastructure, ensuring long-term resilience in an increasingly unpredictable climate.

Data availability statement

The data that support the findings of this study are openly available at the following URL/DOI: https://github.com/devalc/hydroXtremes
Data for the duration, magnitude, and intensity of hydrological extremes at each individual station across different scenarios, seasons, and time periods can be visualized using the application deployed at: https://hydroxtremes.streamlit.app/

Acknowledgements

The authors thank all editors and reviewers who helped improve this manuscript.

References

Aguayo, R., León-Muñoz, J., Garreaud, R., & Montecinos, A. (2021). Hydrological droughts in the southern Andes (40–45°S) from an ensemble experiment using CMIP5 and CMIP6 models. Scientific Reports 2021 11:1, 11(1), 1–16. https://doi.org/10.1038/s41598-021-84807-4

Ali, S., Saeed, A., Kiani, R. S., Muhammad, S., Khan, F., Babar, R., Khan, A., Iqbal, M. S., Goheer, M. A., Naseem, W., & Fahad, S. (2021). Future climatic changes, extreme events, related uncertainties, and policy recommendations in the Hindu Kush sub-regions of Pakistan. Theoretical and Applied Climatology, 143(1–2), 193–209. https://doi.org/10.1007/s00704-020-03399-7

Bosmans, J., Wanders, N., Bierkens, M. F. P., Huijbregts, M. A. J., Schipper, A. M., & Barbarossa, V. (2022). FutureStreams, a global dataset of future streamflow and water temperature. Scientific Data 2022 9:1, 9(1), 1–10. https://doi.org/10.1038/s41597-022-01410-6

Brunner, Manuela I., and Eric Gilleland. 2024. “Future Changes in Floods, Droughts, and Their Extents in the Alps: A Sensitivity Analysis With a Non-Stationary Stochastic Streamflow Generator.” Earth’s Future 12 (4): e2023EF004238. https://doi.org/10.1029/2023EF004238

Campbell, J. L., Driscoll, C. T., Pourmokhtarian, A., & Hayhoe, K. (2011). Streamflow responses to past and projected future changes in climate at the Hubbard Brook Experimental Forest, New Hampshire, United States. Water Resources Research, 47(2), 2514. https://doi.org/10.1029/2010WR009438

Cook, B. I., Mankin, J. S., Marvel, K., Williams, A. P., Smerdon, J. E., & Anchukaitis, K. J. (2020). Twenty-First Century Drought Projections in the CMIP6 Forcing Scenarios. Earth's Future, 8(6), e2019EF001461. https://doi.org/10.1029/2019EF001461

Dankers, R., Arnell, N. W., Clark, D. B., Falloon, P. D., Fekete, B. M., Gosling, S. N., Heinke, J., Kim, H., Masaki, Y., Satoh, Y., Stacke, T., Wada, Y., & Wisser, D. (2014). First look at changes in flood hazard in the Inter-Sectoral Impact Model Intercomparison Project ensemble. *Proceedings of the National Academy of Sciences of the United States of America*, *111*(9), 3257–3261. https://doi.org/10.1073/PNAS.1302078110

de Brito, M. M., Sodoge, J., Fekete, A., Hagenlocher, M., Koks, E., Kuhlicke, C., Messori, G., de Ruiter, M., Schweizer, P. J., & Ward, P. J. (2024). Uncovering the Dynamics of Multi-Sector Impacts of Hydrological Extremes: A Methods Overview. Earth's Future, 12(1), e2023EF003906. https://doi.org/10.1029/2023EF003906

Elgendy, M., Asce, S. M., Hassini, S., Asce, A. M., Coulibaly, P., & Asce, M. (2023). Review of Climate Change Adaptation Strategies in Water Management. Journal of Hydrologic Engineering, 29(1), 03123001. https://doi.org/10.1061/JHYEFF.HEENG-6014

Eyring, V., Bony, S., Meehl, G. A., Senior, C. A., Stevens, B., Stouffer, R. J., & Taylor, K. E. (2016). Overview of the Coupled Model Intercomparison Project Phase 6 (CMIP6) experimental design and organization. Geoscientific Model Development, 9(5), 1937–1958. https://doi.org/10.5194/GMD-9-1937-2016

Falkenmark, M., Wang-Erlandsson, L., & Rockström, J. (2019). Understanding of water resilience in the Anthropocene. Journal of Hydrology X, 2, 100009. https://doi.org/10.1016/J.HYDROA.2018.100009

Gudmundsson, L., Boulange, J., Do, H. X., Gosling, S. N., Grillakis, M. G., Koutroulis, A. G., Leonard, M., Liu, J., Schmied, H. M., Papadimitriou, L., Pokhrel, Y., Seneviratne, S. I., Satoh, Y., Thiery, W., Westra, S., Zhang, X., & Zhao, F. (2021). Globally observed trends in mean and extreme river flow attributed to climate change. Science, 371(6534), 1159–1162. https://www.science.org/doi/10.1126/science.aba3996

Gupta, V., Singh, V., & Jain, M. K. (2020). Assessment of precipitation extremes in India during the 21st century under SSP1-1.9 mitigation scenarios of CMIP6 GCMs. Journal of Hydrology, 590, 125422. https://doi.org/10.1016/J.JHYDROL.2020.125422

GRDC. (2025). Global Runoff Data Center (GRDC) Data Portal. https://portal.grdc.bafg.de/applications/public.html?publicuser=PublicUser#dataDownload/Home (last access: 15 Aug 2025).

Hausfather, Z., Marvel, K., Schmidt, G. A., Nielsen-Gammon, J. W., & Zelinka, M. (2022). Climate simulations: recognize the 'hot model' problem. Nature 2022 605:7908, 605(7908), 26–29. https://doi.org/10.1038/d41586-022-01192-2

Hirabayashi, Y., Mahendran, R., Koirala, S., Konoshima, L., Yamazaki, D., Watanabe, S., Kim, H., & Kanae, S. (2013). Global flood risk under climate change. Nature Climate Change 2013 3:9, 3(9), 816–821. https://doi.org/10.1038/nclimate1911

Hussain, A., Hussain, I., Rezaei, A., Ullah, W., Lu, M., Zhou, J., & Guan, Y. (2024). Increasing monsoon precipitation extremes in relation to large-scale climatic patterns in Pakistan. Atmospheric Research, 309, 107592. https://doi.org/10.1016/J.ATMOSRES.2024.107592

IPCC, 2012: Managing the Risks of Extreme Events and Disasters to Advance Climate Change Adaptation. A Special Report of Working Groups I and II of the Intergovernmental Panel on Climate Change [Field, C.B., V. Barros, T.F. Stocker, D. Qin, D.J. Dokken, K.L. Ebi, M.D. Mastrandrea, K.J. Mach, G.-K. Plattner, S.K. Allen, M. Tignor, and P.M. Midgley (eds.)]. Cambridge University Press, Cambridge, UK, and New York, NY, USA, 582 pp.

IPCC, 2021: Climate Change 2021: The Physical Science Basis. Contribution of Working Group I to the Sixth Assessment Report of the Intergovernmental Panel on Climate Change [Masson-Delmotte, V., P. Zhai, A. Pirani, S.L. Connors, C. Péan, S. Berger, N. Caud, Y. Chen, L. Goldfarb, M.I. Gomis, M. Huang, K. Leitzell, E. Lonnoy, J.B.R. Matthews, T.K. Maycock, T. Waterfield, O. Yelekçi, R. Yu, and B. Zhou (eds.)]. Cambridge University Press, Cambridge, United Kingdom and New York, NY, USA, 2391 pp. https://doi.org/10.1017/9781009157896.

Intergovernmental Panel on Climate Change (IPCC). (2023). Climate Change 2023: Synthesis Report. Contribution of Working Groups I, II and III to the Sixth Assessment Report. In T. H. Lee & J. Romero (Eds.), IPCC. https://www.ipcc.ch/report/ar6/syr/downloads/report/IPCC_AR6_SYR_FullVolume.pdf

Iturbide, M., Gutiérrez, J. M., Alves, L. M., Bedia, J., Cerezo-Mota, R., Cimadevilla, E., Cofiño, A. S., Luca, A. di, Faria, S. H., Gorodetskaya, I. v., Hauser, M., Herrera, S., Hennessy, K., Hewitt, H. T., Jones, R. G., Krakovska, S., Manzanas, R., Martínez-Castro, D., Narisma, G. T., … Vera, C. S. (2020). An update of IPCC climate reference regions for subcontinental analysis of climate model data: definition and aggregated datasets. Earth System Science Data, 12(4), 2959–2970. https://doi.org/10.5194/ESSD-12-2959-2020

John, A., Douville, H., Ribes, A., & Yiou, P. (2022). Quantifying CMIP6 model uncertainties in extreme precipitation projections. Weather and Climate Extremes, 36, 100435. https://doi.org/10.1016/J.WACE.2022.100435

Khan, F., Ali, S., Ullah, H., & Muhammad, S. (2023). Twenty-first century climate extremes' projections and their spatio-temporal trend analysis over Pakistan. Journal of Hydrology: Regional Studies, 45, 101295. https://doi.org/10.1016/j.ejrh.2022.101295

Lehner, B., Liermann, C. R., Revenga, C., Vörömsmarty, C., Fekete, B., Crouzet, P., Döll, P., Endejan, M., Frenken, K., Magome, J., Nilsson, C., Robertson, J. C., Rödel, R., Sindorf, N., & Wisser, D. (2011). High-resolution mapping of the world's reservoirs and dams for sustainable river-flow management. Frontiers in Ecology and the Environment, 9(9), 494–502. https://doi.org/10.1890/100125

Lei, Y., Chen, J., & Xiong, L. (2023). A comparison of CMIP5 and CMIP6 climate model projections for hydrological impacts in China. Hydrology Research, 54(3), 330–347. https://doi.org/10.2166/NH.2023.108

Li, Z., Smerdon, J. E., Seager, R., Siegert, N., & Mankin, J. S. (2024). Emergent Trends Complicate the Interpretation of the United States Drought Monitor (USDM). AGU Advances, 5(2), e2023AV001070. https://doi.org/10.1029/2023AV001070

Martel, J. L., Brissette, F., Troin, M., Arsenault, R., Chen, J., Su, T., & Lucas-Picher, P. (2022). CMIP5 and CMIP6 Model Projection Comparison for Hydrological Impacts Over North America. Geophysical Research Letters, 49(15), e2022GL098364. https://doi.org/10.1029/2022GL098364

Matanó, A., Berghuijs, W. R., Mazzoleni, M., de Ruiter, M. C., Ward, P. J., & van Loon, A. F. (2024). Compound and consecutive drought-flood events at a global scale. Environmental Research Letters, 19(6), 064048. https://doi.org/10.1088/1748-9326/AD4B46

Milly, P. C. D., Betancourt, J., Falkenmark, M., Hirsch, R. M., Kundzewicz, Z. W., Lettenmaier, D. P., & Stouffer, R. J. (2008). Climate change: Stationarity is dead: Whither water management? Science, 319(5863), 573–574. https://doi.org/10.1126/science.1151915

Raymond, C., Horton, R. M., Zscheischler, J., Martius, O., AghaKouchak, A., Balch, J., Bowen, S. G., Camargo, S. J., Hess, J., Kornhuber, K., Oppenheimer, M., Ruane, A. C., Wahl, T., & White, K. (2020). Understanding and managing connected extreme events. Nature Climate Change 2020 10:7, 10(7), 611–621. https://doi.org/10.1038/s41558-020-0790-4

Sutanudjaja, E. H., van Beek, R., Wanders, N., Wada, Y., Bosmans, J. H. C., Drost, N., van der Ent, R. J., de Graaf, I. E. M., Hoch, J. M., de Jong, K., Karssenberg, D., López López, P., Peßenteiner, S., Schmitz, O., Straatsma, M. W., Vannametee, E., Wisser, D., & Bierkens, M. F. P. (2018). PCR-GLOBWB 2: A 5 arcmin global hydrological and water resources model. Geoscientific Model Development, 11(6), 2429–2453. https://doi.org/10.5194/GMD-11-2429-2018

van Beek, L. P. H., Eikelboom, T., van Vliet, M. T. H., & Bierkens, M. F. P. (2012). A physically based model of global freshwater surface temperature. Water Resources Research, 48(9). https://doi.org/10.1029/2012WR011819

van der Wiel, K., Wanders, N., Selten, F. M., & Bierkens, M. F. P. (2019). Added Value of Large Ensemble Simulations for Assessing Extreme River Discharge in a 2 °C Warmer World. Geophysical Research Letters, 46(4), 2093–2102. https://doi.org/10.1029/2019GL081967

Warszawski, L., Frieler, K., Huber, V., Piontek, F., Serdeczny, O., & Schewe, J. (2014). The inter-sectoral impact model intercomparison project (ISI-MIP): Project framework. Proceedings of the National Academy of Sciences of the United States of America, 111(9), 3228–3232. https://doi.org/10.1073/pnas.1312330110

Zhai, J., Mondal, S. K., Fischer, T., Wang, Y., Su, B., Huang, J., Tao, H., Wang, G., Ullah, W., & Uddin, M. J. (2020). Future drought characteristics through a multi-model ensemble from CMIP6 over South Asia. Atmospheric Research, 246, 105111. https://doi.org/10.1016/J.ATMOSRES.2020.105111

Zhang, S., & Chen, J. (2021). Uncertainty in Projection of Climate Extremes: A Comparison of CMIP5 and CMIP6. Journal of Meteorological Research, 35(4), 646–662. https://doi.org/10.1007/S13351-021-1012-3

Zheng, H., Chiew, F. H. S., Post, D. A., Robertson, D. E., Charles, S. P., Grose, M. R., & Potter, N. J. (2024). Projections of future streamflow for Australia informed by CMIP6 and previous

generations of global climate models. Journal of Hydrology, 636, 131286. https://doi.org/10.1016/J.JHYDROL.2024.131286

Zscheischler, J., Martius, O., Westra, S., Bevacqua, E., Raymond, C., Horton, R. M., van den Hurk, B., AghaKouchak, A., Jézéquel, A., Mahecha, M. D., Maraun, D., Ramos, A. M., Ridder, N. N., Thiery, W., & Vignotto, E. (2020). A typology of compound weather and climate events. Nature Reviews Earth & Environment 2020 1:7, 1(7), 333–347. https://doi.org/10.1038/s43017-020-0060-z